Nanoscale

Cite this: *Nanoscale*, 2012, **4**, 5425

www.rsc.org/nanoscale

PAPER

Controllable synthesis of monodisperse ultrathin SnO_2 nanorods on nitrogen-doped graphene and its ultrahigh lithium storage properties†

Chaohe Xu, Jing Sun* and Lian Gao*

Received 1st June 2012, Accepted 1st July 2012
DOI: 10.1039/c2nr31357j

Monodisperse ultrathin SnO_2 nanorods on nitrogen-doped graphene were firstly synthesized by a facile one-step hydrothermal strategy. The uniformed composites with high nitrogen content and ultrathin SnO_2 nanorods of 2.5–4.0 nm in diameter and 10–15 nm in length show a high reversible specific capacity, superior rate capability and outstanding cycling stability (803 mA h g^{-1}) as anode materials for lithium ion batteries, owing to the synergistic effect between GS and SnO_2 and nitrogen-doping, which can greatly decrease the energy barrier for Li penetrating the pyridinic defects and improve the electronic structures. This work opens the door to prepare metal oxide/GS-N composites with superior lithium storage properties and engineering of graphene composites for advanced energy storage.

Introduction

Recently, there has been a great increase in demand for clean and efficient energy storage devices due to the ever-rising concerns about the limited global energy supply and environment and climate change.[1,2] Due to their high energy density, rechargeable lithium ion batteries (LIBs) have become one of the dominant power sources for human beings. However, the energy and power densities of LIBs require significant improvement in order to fulfil the new demands of the future, such as powering electric vehicles and long-term electronics, which can only be achieved by making a breakthrough in electrode materials.[2,3] Therefore, it is highly desirable to develop new anode materials to replace the widely used graphite materials with a theoretical capacity of only 372 mA h g^{-1}. Tin oxide (SnO_2), an n-type semiconductor, has been regarded as a potential anode material for LIBs owing to its high theoretical specific capacity (~782 mA h g^{-1}). However, the large volume effect (>300%) during lithium insertion and extraction processes greatly limit its wide application in rechargeable LIBs due to electrode pulverization and loss of electrical contact with current collectors.[4,5] In order to solve these problems, composites based on SnO_2 have been widely investigated for their potential to integrate the unique properties of both components, such as SnO_2/Fe_2O_3, SnO_2/In_2O_3 and SnO_2/graphite.[6–10] According to these, carbonaceous materials have attracted considerable interest owing to their high electrical conductivity, large surface area and superior mechanical properties.[4,8] For instance, monodisperse SnO_2/carbon colloids have been synthesized as anode materials for LIBs and exhibited values as high as 440 mA h g^{-1} after 100 cycles.[11] In addition, SnO_2 nanostructures have been rationally designed as hollow carbon spheres which deliver a stable capacity of about 500 mA h g^{-1} for at least 200 cycles.[12] Though hybridizing SnO_2 with carbon is effective, this approach sacrifices the theoretical capacity itself due to introduction of carbon and is usually complicated in fabrication.[5]

Graphene, a monolayer of carbon atoms arranged in a honeycomb network, can stably store lithium on both sides of the graphene sheet and has a theoretical capacity of 744 mA h g^{-1}.[13–15] It has drawn intensive attention in rechargeable LIBs due to its unique electrical and mechanical properties, large surface area and high chemical stability.[15–17] However, its ultra large capacity loss in the electrochemical cycles (capacity retention is only ~20%) is very similar to other pure carbon nanomaterials.[18–20] Recently, some research results demonstrated that chemical doping such as nitrogen-doping[21,22] and hybridizing with nanoparticles[23–25] were effective ways to improve the electrochemical properties of graphene. For example, the reversible discharge capacity of N-doped graphene grown on Cu current collectors is almost double compared to that of pristine graphene.[26] Similar results have been also demonstrated in the research of Cui and coworkers, where the N-doped graphene delivered a higher reversible capacity of ~900 mA h g^{-1} at a current density of 42 mA g^{-1} and an improved rate capability compared to that of pristine graphene.[27] On the other hand, composites with nanoparticles, such as Fe_3O_4, Co_3O_4 and SnO_2, have also been recently prepared as anode materials and exhibited enhanced performance.[25,28–32] For instance, nanoporous SnO_2/GS composites were synthesized by an interface reassembled method and retained a specific capacity of 570 mA h g^{-1} after 15 cycles at 60 mA g^{-1}.[31] Liu and coworkers have

The State Key Lab of High Performance Ceramics and Superfine Microstructure, Shanghai Institute of Ceramics, Chinese Academy of Sciences, 1295 Dingxi Road, Shanghai 200050, P. R. China. E-mail: jingsun@mail.sic.ac.cn; liagao@mail.sic.ac.cn; Fax: +86-21-52413122; Tel: +86-21-52414301

† Electronic supplementary information (ESI) available: XRD, TEM, SEM, TG-DTA and XPS. See DOI: 10.1039/c2nr31357j

developed a ternary self-assembly approach using GS as fundamental building blocks to construct ordered SnO_2/GS composites, which showed a steady specific capacity of 625 mA h g^{-1} at 10 mA g^{-1} after 10 cycles.[32] Considering the previous literature in which nitrogen-doping of GS and composites with nanocrystals on GS can greatly improve the lithium storage properties, we deduce that hybrids of nitrogen-doped GS and nanoparticles might can be superior anode materials for LIBs. However, in these reports, strong reducing agents such as hydrazine and sodium borohydride were widely used in the chemical reduction of GO to GS. Considering the toxicity and risk of such strong reducing reagents, it is highly desirable to develop a green chemical route for the synthesis of nanocrystals on GS with high conductivity and controllable morphology. As far as we know, there are few reports on preparing monodisperse nanocrystals with specific morphology on nitrogen-doped graphene directly from GO suspension; though preparing metal oxide nanocrystals on graphene as anode materials for LIBs has been widely investigated. On the other hand, unlike the homogeneous solution, the physical morphology and crystallinity of nanocrystals can be easily controlled in nucleation and growth processes; it is more difficult to synthesise nanocrystals with specific controllable morphologies in heterogeneous nucleation processes. Although metal oxide nanowires and nanoarrays attached on GS have been reported and applied as anode materials for LIBs, it is still very challenging to explore a green and facile chemical route for the direct synthesis of nanocrystals with specific morphology on GS.

We herein develop a novel one-step strategy to direct synthesize monodisperse ultrathin SnO_2 nanorods on nitrogen-doped graphene with controllable crystallinity and morphology. The hybrids possess several advantages: First, ultrathin SnO_2 nanorods enable effective electrolyte transport, active-site accessibility and good electron transportation between GS-N and SnO_2. Second, the ultrathin nanostructures can well accommodate the volume effects of SnO_2 in lithium insertion and extraction process. Third, nitrogen doping can greatly improve the electronic structure of graphene, decrease the energy barrier for Li penetrating the defects and enhance the lithium storage properties. Fourth, the method can be easily scaled up and provide a new way to decorate nanocrystals on nitrogen-doped graphene. To our knowledge, this is the first time that ultrathin metal oxide nanorods have been directly grown on nitrogen-doped graphene by a facile solution method.

Experimental

Materials

Graphite was purchased from Alfa Aesar (−325 mesh). All chemicals were of analytic grade and used without further purification.

Synthesis of SnO_2/GS-N composites

GO was prepared from graphite flakes by a modified Hummers method.[33,34] The composites of ultrathin SnO_2 nanorods on GS-N were synthesized simply by a direct hydrothermal method. Briefly, 50 mg of stannic chloride hydrate was dissolved into 40 mL of a 1 mg mL^{-1} GO aqueous dispersion and vigorously stirred for 10 min. Afterwards, 1.0 g of urea and 2 mL of concentrated HCl were added to the above suspension. Then, the suspension was transferred to a 50 mL Teflon lined stainless steel autoclave for hydrothermal reaction at 120 °C for 24 h.

Characterization methods

Transmission electron microscopy (TEM) was performed on a JEM-2100F Electron Microscope with an accelerating voltage of 200 kV. Field-emission scanning electron microscope (FE-SEM) was performed on JSM-6700F at an acceleration voltage of 10.0 kV. Raman spectra were recorded on a DXR Raman Microscope with 532 nm excitation length, Thermal Scientific Co., USA, respectively.

The electrochemical properties of the SnO_2/GS composites as the negative electrode used in Li-ion batteries were characterized at room temperature. The working electrode was prepared from the mixture of the active materials, carbon black and polyvinylidene fluoride (PVDF) binder in weight ratio of 80 : 10 : 10. Li foil was used as the counter electrode. The electrolyte was 1 M LiPF6 in a 50 : 50 w/w mixture of ethylene carbonate (EC) and dimethyl carbonate (DMC). Cell assembly was carried out in glove box with a concentration of moisture and oxygen below 1 ppm. The batteries were measured using a CT2001 battery tester.

Results and discussions

The composites of monodispersed ultrathin SnO_2 nanorods on nitrogen-doped graphene are prepared by direct hydrothermal reaction at 120 °C for 24 h. Graphene oxide (GO) is prepared by the modified Hummer's method.[34] After hydrothermal reaction, a broad peak at ~25° appeared, indicating the reduction of GO as shown in Fig. 1 (black). The XRD patterns of the composites clearly show the good crystallization of tetragonal SnO_2 (*t*-SnO_2, JCPDS card no. 41-1445; red curve in Fig. 1 and Fig. S1†). The diffraction peak of GS at 25° overlapped with the (110) peak of SnO_2. The mean particle size of SnO_2 nanorods calculated by the Scherrer equation is ~3.6 nm based on the (110) diffraction peak, which is consistent with that of the transmission electron

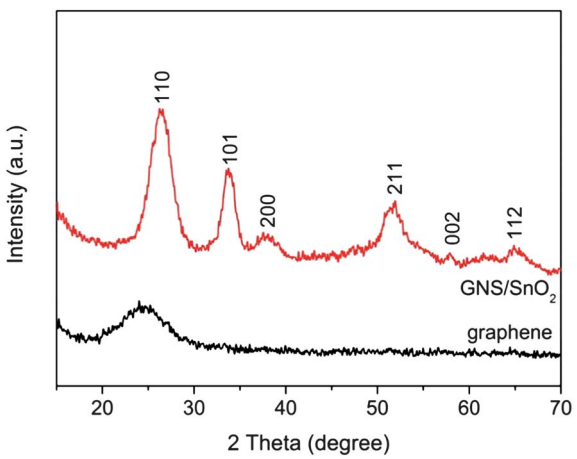

Fig. 1 XRD curves of the as synthesized GS and SnO_2/GS-N composites.

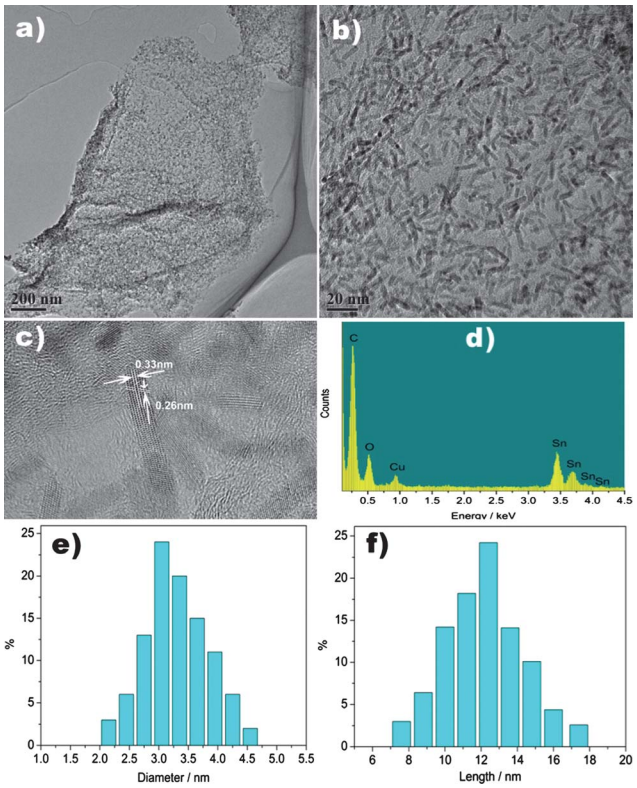

Fig. 2 (a and b) Low and high magnifications TEM images of the ultrathin SnO_2 nanorods on GS. (c) High-resolution TEM image of the ultrathin SnO_2 nanorods on GS. (d) X-Ray energy-dispersive spectroscopy of the SnO_2/GS-N composites. (e and f) The statistical sizes of the ultrathin SnO_2 nanorods.

microscopy (TEM) images (Fig. 2a–c). Additional TEM images are shown in Fig. S2 and S3,† which exhibit detailed morphology changes on the nanocrystals. The SnO_2 nanorods were monodisperse and uniformly decorated on the surface of the GS with sizes of 2.5–4.0 nm in diameter and 10–15 nm in length. These coincide well with the statistical results of the sizes of SnO_2 nanorods (Fig. 2e and f). Composition and detailed structure of the SnO_2 nanorods and the composites have been characterized using X-ray energy-dispersive spectroscopy (EDS) and high resolution transmission electron microscopy (HRTEM). An HRTEM image (Fig. 2c) shows that the crystal lattice fringes is 0.33 and 0.26 nm, corresponding to the (110) and (101) face of *t*-SnO_2. Its elemental composition is verified by EDS (Fig. 2d) as Sn and O with an approximate atomic ratio of 1 : 2.6 (the Cu and C signals come from the TEM grids and GS, respectively). The excessive oxygen comes from the functional groups of GS which is not completely reduced by hydrothermal dehydration. Fig. S4† exhibits the thermal stability of SnO_2/GS using thermogravimetric (TG) analysis. The weight loss of 9.87 wt% around 100 °C and weight loss of 41.49 wt% between 200 and 550 °C were ascribed to the loss of absorbed water and the pyrolysis of GS, respectively. The mass loading of SnO_2 calculated was 62.6 wt% in the SnO_2/GS composites.

To characterize the composites in detail, X-ray photoelectron spectroscopy (XPS) and Raman spectra were used to determine the electronic and compositions. The XPS spectrum show the

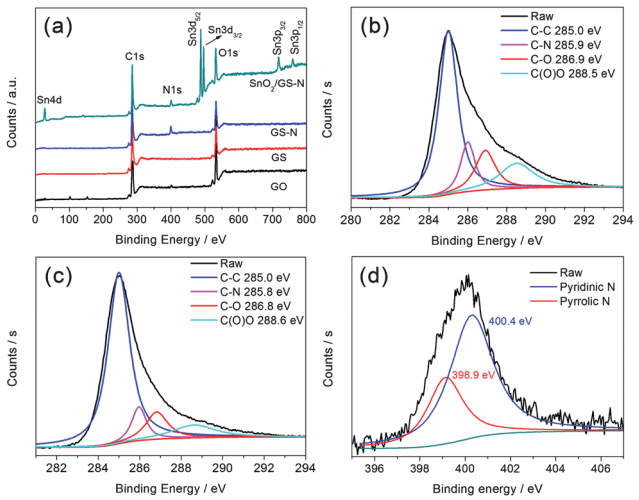

Fig. 3 (a) The XPS curves of GO, GS, GS-N and SnO_2/GS-N composites. (b) The deconvoluted C1s of GS-N and C1s of SnO_2/GS-N (c) and N1s of SnO_2/GS-N composites (d).

existence of C, O, and Sn in the SnO_2/GS-N composites (Fig. 3a), which was consistent with the EDS analysis mentioned above. It is noteworthy that nitrogen is also detected in the spectra of GS-N and SnO_2/GS-N. This verified that N was successfully doped into the composites. Fig. 3b and c shows the deconvoluted C1s spectra of GS-N and SnO_2/GS-N, respectively. The peaks centered at 285.0, 285.8, 286.8 and 288.6 eV were attributed to the C–C, C–N, C–O and C(O)O, respectively.[35,36] The N1s peak can be split into two Lorentzian peaks as shown in Fig. 3d. Nitrogen atoms in the SnO_2/GS-N exist as pyrrolic and pyridinic nitrogen atoms, corresponding to binding energy peaks at 398.9 and 400.4 eV, respectively.[21,27] A doping level of 4.6% nitrogen was detected and the N binding configuration includes 30.7% pyrrolic N and 69.3% pyridinic N. Detailed XPS data are shown in Table 1 and Fig. S5.† Theoretical investigations showed that the coexistence of vacancy and electron deficiency at the pyridinic-like defects can provide a feasible pathway for Li penetration of the graphene-layers.[37] Therefore, nitrogen-doping is beneficial for improving lithium storage properties. As shown in Fig. 4, the G bands of the SnO_2/GS-N composites (1601.9 cm^{-1}) and GS-N (1596.9 cm^{-1}) exhibit blue shifts compared with GO and GS, which revealed the p-type doping effect on GS (electron withdrawing effect).[34,38] These revealed the electronic interactions between SnO_2 nanorods and GS, which are beneficial for electron transportation between SnO_2 and GS and the formation of three-dimensional electron networks, which is desirable for lithium storage. And also, a prominent D band is an indication of disordered carbon structure in GS, originating from defects

Table 1 The elements content and C/O ratios of GO, GS, GS-N and composites of SnO_2/GS-N

Sample	C	O	N	C/O
GO	67.6	32.1	0.4	2.1
GS	81.6	18	0.4	4.5
GS-N	74.9	19.2	6.63	3.9
SnO_2/GS-N	70.3	19.6	4.6	3.6

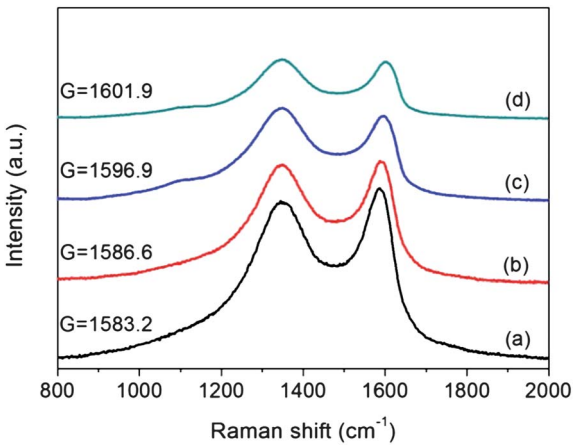

Fig. 4 Raman spectra of (a) GO, (b) GS, (c) GS-N and (d) SnO_2/GS-N composites.

associated with vacancies, grain boundaries and amorphous carbon species. The intensity ratio (I_D/I_G) of the D band to the G band is related to the extent of π-conjugation and the concentration of defects, which are 1.23, 1.32, 1.56 and 1.51, respectively, for GO, GS, GS-N and SnO_2/GS-N. The large I_D/I_G ratio indicates a high concentration of structure defects exist on the surface of graphene. As we all know, the defects of graphene can provide more active sites for lithium storage, which can greatly enhance the properties of the composites. Therefore, the hybrids are expected to be a promising candidate for high-capacity anodes for lithium ion batteries.

Coin cells were made to test the electrochemical performance of SnO_2/GS-N composites as anode materials and with Li foil as counter electrode. Fig. 5a–c shows the typical discharge and charge curves of the composites at current densities of 100, 200 and 1000 mA g^{-1}, respectively. The capacity corresponding to voltage range of ~1.0 to 0.5 V of the first Li^+ discharge curves can be attributed to the irreversible reaction of the formation of SEI layer, which delivers capacities of ~800, ~600 and ~200 mA h g^{-1}. The charge curves show a sloping plateau at ~1.25 V due to the partially reversible reaction of the formation of the SEI layer. As shown in Fig. 5a, the initial discharge and charge capacities are 1996 and 1144.5 mA h g^{-1} at a current density of 100 mA g^{-1}. When the current density increased to 200 mA g^{-1} (Fig. 5b), the discharge and charge capacities are 1491.9 and 844 mA h g^{-1}, respectively. The Coulombic efficiencies are 57.3 and 56.6%, respectively. Even at a current density of 1000 mA g^{-1}, our materials still exhibit an initial discharge capacity of 837.4 mA h g^{-1}. These values indicate that our materials can exhibit superior lithium storage properties. After 30 cycles, the discharge capacities are 974.1, 810.4 and 562.1 mA h g^{-1} at current densities of 100, 200 and 1000 mA g^{-1}, respectively. The Coulombic efficiencies of our materials increase higher than 98.5% after 10 cycles, indicating the good reversibility of the lithium insertion and extraction reactions. To date, as far as we know, these results outperform many other currently available SnO_2 and SnO_2/GS composites.

Fig. 5d shows the cycling performance of the SnO_2/GS-N composites at different current densities. The second discharge capacities are 1182, 914.8 and 676.2 mA h g^{-1} at current densities of 100, 200 and 1000 mA g^{-1}, respectively, which retained about 59.2, 61.3 and 80.7% of the initial discharge capacities. After 50 cycles, the discharge capacities are 900.8, 773.5 and 505.5 mA h g^{-1} and the capacity loss is ~0.4% per cycle at current density of 100 and 200 mA g^{-1} and ~0.2% at 1000 mA g^{-1}, respectively. Prolonging this to 100 cycles, the reversible discharge capacities remain as high as 803.1 and 773.5 mA h g^{-1} at current densities of 100 and 200 mA g^{-1}. As far as we know, the cyclic performances

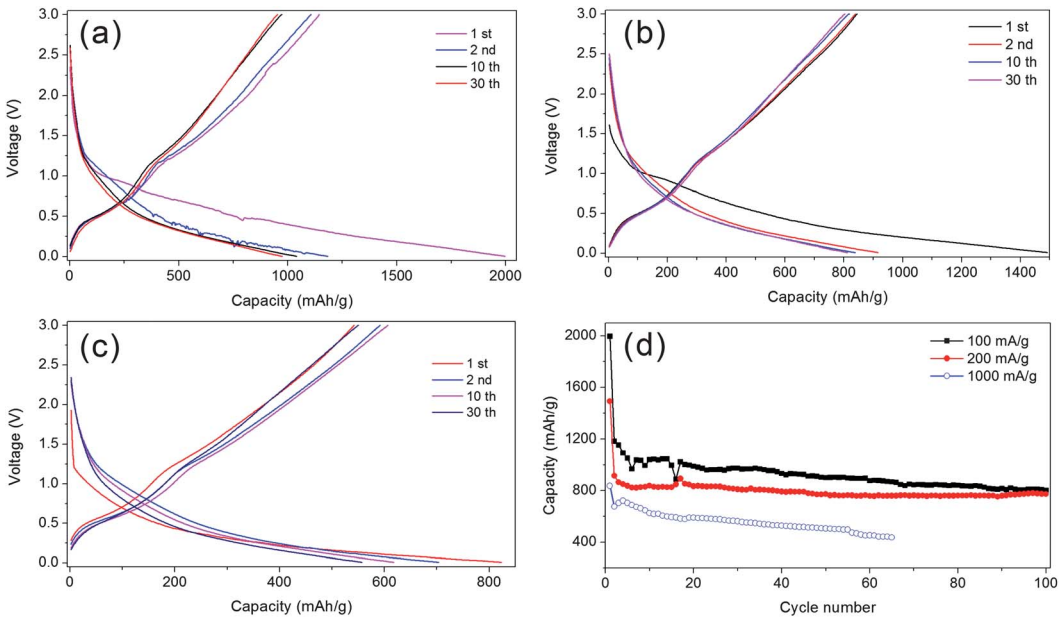

Fig. 5 (a–c) The discharge–charge profiles of the ultrathin SnO_2 nanorods/GS-N composites at current densities of 100, 200 and 1000 mA g^{-1}, respectively. (d) Cycling performance of SnO_2/GS-N composites in 5 mV–3 V (*vs.* Li^+/Li) voltage window at current density of 100, 200 and 1000 mA g^{-1}, respectively.

are almost superior to all of the SnO_2 nanoparticles coated on carbon nanotubes or encapsulated in carbon spheres,[4,8,11,12] especially at high current densities of 1000 mA g^{-1}. This is attributed to the intimate interactions between GS substrates and the SnO_2 nanorods directly grown on them, which could effectively and rapidly transport electrons between SnO_2 and GS to the current collector through the highly conducting three-dimensional GS network.

Fig. 6a shows the representative discharge and charge voltage profiles of the same cell at various current densities. With increasing current densities, the discharge potential of our materials decreased and the charge potential increased. The cell was first cycled at a current density of 50 mA g^{-1}. It showed a very high specific capacity of ~1739.4 and 1028 mA h g^{-1} in the first cycle based on the total mass of the composites, as shown in Fig. 6a (red curves). These are larger than the theoretical capacity of SnO_2 (~782 mA h g^{-1}) and our SnO_2/GS-N composites ($C_{theo.} = C_{SnO2} \times \%_{SnO2} + C_{GS} \times \%_{GS} = 782 \times 0.626 + 774 \times 0.374 = 767.8$ mA h g^{-1}; here, we regard the theoretical capacity of single layer graphene as 774 mA h g^{-1}, which is related to the electrochemical reaction of $Li_2C_6 = C_6 + 2Li^+ + 2e$).[15] The observed capacity of the SnO_2/GS-N is comparable to the theoretical capacity even at a current density of 200 mA g^{-1} after 50 cycles, highlighting the synergetic effect on the enhanced cyclic performance. When the current density increased to 400 mA g^{-1}, our materials remain able to deliver discharge capacities of 697.8 mA h g^{-1}, almost ~90% of the theoretical capacity of the composites. The lithium storage properties of the hybrid electrodes are superior to the ternary self-assembly of ordered SnO_2/GS composites, SnO_2/GS nanoporous composites prepared by reassembled process and *in situ* chemical methods.[31,32,39–41] The high reversible discharge capacity compared with the other tin oxide composites can be attributed to the topological defects of our materials. First, a large number of surface defects were introduced onto the graphene sheet during chemical exfoliation and the N-doping process, which led to the formation of disordered carbon structure that further increases the active sites for Li storage and enhances Li intercalation properties.[26] As observed in the XPS data, our materials have a high percentage of pyridinic N present. Theoretical studies illustrated that the pyridinic N in carbon materials could apparently reduce the energy barrier for Li penetrating the carbon layers.[37] The energy barrier for Li penetrating the pyridinic defect is about ~1.44 eV, much lower than those penetrating the perfect graphene layers.[37] As we all know, lithium storage is also a kinetic process, and the existence of vacancies and electron deficiencies in pyridinic N provides a feasible pathway for Li penetration of the graphene layers. Therefore, the pyridinic N atoms could also be involved in the high reversible capacity of the materials.

Fig. 6b show the capacity retention and Coulombic efficiency of our materials at various current densities for the same cell. A relatively high and stable specific capacity of ~1026 mA h g^{-1} was obtained in the first five cycles at 50 mA g^{-1}. Continuing to 20 or 50 cycles at 100 and 200 mA g^{-1}, the cell can deliver very high capacities of 892.1 and 755 mA h g^{-1}, respectively. Further increasing the current density to 400 mA g^{-1}, a stable reversible capacity of 642 mA h g^{-1} and a high Coulombic retention of 99.2% were obtained at the 80th cycle. To the best of our knowledge, these are almost the highest capacities that has been reported for SnO_2 anode materials. Notably, the Coulombic retention of our materials increased with increasing current density (from 96.1% at 50 mA g^{-1} to 97.2% at 100 mA g^{-1}, 98.5% at 200 mA g^{-1} and 99.2% at 400 mA g^{-1}; all are average values).

As mentioned by many other researches, the main disadvantage of SnO_2 based electrodes is that a larger volume expansion of SnO_2 occurs during the cycling and leads to pulverization of the electrode.[4,5,8,12] For our SnO_2/GS-N composites, the ultrathin tin oxide nanorods are uniformly distributed on the surface of nitrogen-doped graphene. Such hybrid structure can limit the larger volume expansion upon lithium insertion and avoid the pulverization of electrode materials and loss of contact with the current collector. Even though volume effects occurred, the electrode was not pulverized because our materials have enough void space to buffer the volume changes. Another important reason for the superior cyclic stability is the nanoscale effect of the ultrathin SnO_2 nanorods. Previous studies illustrated that the nanoscale structures can accommodate the strain stress much better than the films and bulk materials, which can release the stress occurring in the lithium insertion and extraction process. These factors lead to enhanced lithium storage properties and superior cyclic stability. Furthermore, graphene nanosheets in our materials could act as not only lithium storage electrodes but also as electronic conductive channels to improve electrochemical performance.

Conclusions

In summary, monodisperse ultrathin SnO_2 nanorods on nitrogen-doped graphene were synthesized for the first time by a novel one-step hydrothermal strategy. The uniform composites

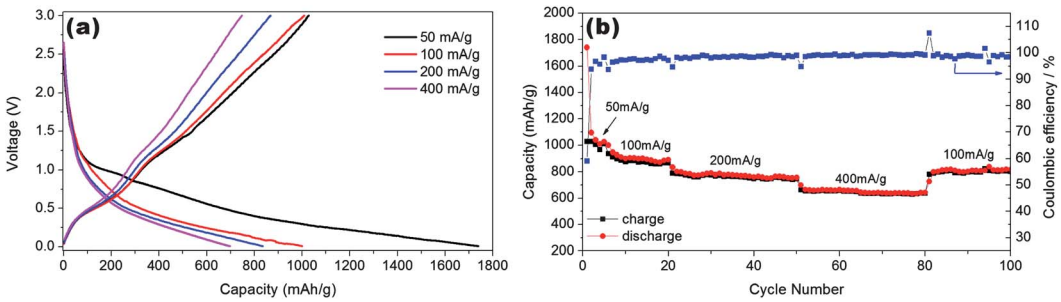

Fig. 6 (a) Representative discharge–charge curves of ultrathin SnO_2 nanorods/GS-N composites at various current densities. (b) Capacity retention of ultrathin SnO_2 nanorods/GS-N composites at various current densities.

with high nitrogen content showed a high specific capacity, superior rate capability and cycling stability, owing to the synergistic effect between the GS and the SnO_2 nanorods and the nitrogen doping which can greatly decrease the energy barrier for Li to penetrate the pyridinic moieties and improve the electronic structure. This work opens the door to prepare metal oxide/GS-N composites with superior lithium storage properties and engineer graphene composites for advanced energy storage.

Acknowledgements

This work is supported by the National Natural Science Foundation of China (Grant no. 50972153, 509721157 and 51072215) and Shanghai Municipal Committee of Science and Technology (Grant no. 10DZ0505000).

Notes and references

1 K. S. Kang, Y. S. Meng, J. Breger, C. P. Grey and G. Ceder, *Science*, 2006, **311**, 977–980.
2 A. S. Arico, P. Bruce, B. Scrosati, J. M. Tarascon and W. Van Schalkwijk, *Nat. Mater.*, 2005, **4**, 366–377.
3 J. M. Tarascon and M. Armand, *Nature*, 2001, **414**, 359–367.
4 C. H. Xu, J. Sun and L. Gao, *J. Phys. Chem. C*, 2009, **113**, 20509–20513.
5 C. Wang, Y. Zhou, M. Y. Ge, X. B. Xu, Z. L. Zhang and J. Z. Jiang, *J. Am. Chem. Soc.*, 2010, **132**, 46–47.
6 J. S. Chen, C. M. Li, W. W. Zhou, Q. Y. Yan, L. A. Archer and X. W. Lou, *Nanoscale*, 2009, **1**, 280–285.
7 D. W. Kim, I. S. Hwang, S. J. Kwon, H. Y. Kang, K. S. Park, Y. J. Choi, K. J. Choi and J. G. Park, *Nano Lett.*, 2007, **7**, 3041–3045.
8 Y. J. Chen, C. L. Zhu, X. Y. Xue, X. L. Shi and M. S. Cao, *Appl. Phys. Lett.*, 2008, **92**.
9 Y. Wang and J. Y. Lee, *Electrochem. Commun.*, 2003, **5**, 292–296.
10 Y. Wang and J. Y. Lee, *J. Power Sources*, 2005, **144**, 220–225.
11 X. W. Lou, J. S. Chen, P. Chen and L. A. Archer, *Chem. Mater.*, 2009, **21**, 2868–2874.
12 X. W. Lou, C. M. Li and L. A. Archer, *Adv. Mater.*, 2009, **21**, 2536–2539.
13 X. Y. Han, G. Y. Qing, J. T. Sun and T. L. Sun, *Angew. Chem., Int. Ed.*, 2012, **51**, 5147–5151.
14 A. Gerouki, M. A. Goldner, R. B. Goldner, T. E. Haas, T. Y. Liu and S. Slaven, *J. Electrochem. Soc.*, 1996, **143**, L262–L263.
15 G. X. Wang, B. Wang, X. L. Wang, J. Park, S. X. Dou, H. Ahn and K. Kim, *J. Mater. Chem.*, 2009, **19**, 8378–8384.
16 S. Stankovich, D. A. Dikin, G. H. B. Dommett, K. M. Kohlhaas, E. J. Zimney, E. A. Stach, R. D. Piner, S. T. Nguyen and R. S. Ruoff, *Nature*, 2006, **442**, 282–286.
17 D. A. Dikin, S. Stankovich, E. J. Zimney, R. D. Piner, G. H. B. Dommett, G. Evmenenko, S. T. Nguyen and R. S. Ruoff, *Nature*, 2007, **448**, 457–460.
18 C. Y. Wang, D. Li, C. O. Too and G. G. Wallace, *Chem. Mater.*, 2009, **21**, 2604–2606.
19 A. V. Murugan, T. Muraliganth and A. Manthiram, *Chem. Mater.*, 2009, **21**, 5004–5006.
20 D. S. Zheng, S. X. Sun, W. L. Fan, H. Y. Yu, C. H. Fan, G. X. Cao, Z. L. Yin and X. Y. Song, *J. Phys. Chem. B*, 2005, **109**, 16439–16443.
21 X. L. Li, H. L. Wang, J. T. Robinson, H. Sanchez, G. Diankov and H. J. Dai, *J. Am. Chem. Soc.*, 2009, **131**, 15939–15944.
22 Y. F. Tang, B. L. Allen, D. R. Kauffman and A. Star, *J. Am. Chem. Soc.*, 2009, **131**, 13200–13201.
23 D. H. Wang, D. W. Choi, J. Li, Z. G. Yang, Z. M. Nie, R. Kou, D. H. Hu, C. M. Wang, L. V. Saraf, J. G. Zhang, I. A. Aksay and J. Liu, *ACS Nano*, 2009, **3**, 907–914.
24 A. N. Cao, Z. Liu, S. S. Chu, M. H. Wu, Z. M. Ye, Z. W. Cai, Y. L. Chang, S. F. Wang, Q. H. Gong and Y. F. Liu, *Adv. Mater.*, 2010, **22**, 103–106.
25 C. Xu, J. Sun and L. Gao, *J. Mater. Chem.*, 2012, **22**, 975–979.
26 A. L. M. Reddy, A. Srivastava, S. R. Gowda, H. Gullapalli, M. Dubey and P. M. Ajayan, *ACS Nano*, 2010, **4**, 6337–6342.
27 H. Wang, C. Zhang, Z. Liu, L. Wang, P. Han, H. Xu, K. Zhang, S. Dong, J. Yao and G. Cui, *J. Mater. Chem.*, 2011, **21**, 5430–5434.
28 G. M. Zhou, D. W. Wang, F. Li, L. L. Zhang, N. Li, Z. S. Wu, L. Wen, G. Q. Lu and H. M. Cheng, *Chem. Mater.*, 2010, **22**, 5306–5313.
29 J. Z. Wang, C. Zhong, D. Wexler, N. H. Idris, Z. X. Wang, L. Q. Chen and H. K. Liu, *Chem.–Eur. J.*, 2011, **17**, 661–667.
30 Z. S. Wu, W. C. Ren, L. Wen, L. B. Gao, J. P. Zhao, Z. P. Chen, G. M. Zhou, F. Li and H. M. Cheng, *ACS Nano*, 2010, **4**, 3187–3194.
31 S. M. Paek, E. Yoo and I. Honma, *Nano Lett.*, 2009, **9**, 72–75.
32 D. H. Wang, R. Kou, D. Choi, Z. G. Yang, Z. M. Nie, J. Li, L. V. Saraf, D. H. Hu, J. G. Zhang, G. L. Graff, J. Liu, M. A. Pope and I. A. Aksay, *ACS Nano*, 2010, **4**, 1587–1595.
33 Y. Chen, X. Zhang, P. Yu and Y. W. Ma, *Chem. Commun.*, 2009, 4527–4529.
34 C. H. Xu, J. Sun and L. Gao, *J. Mater. Chem.*, 2011, **21**, 11253–11258.
35 Z. Li, Y. Mi, X. Liu, S. Liu, S. Yang and J. Wang, *J. Mater. Chem.*, 2011, **21**, 14706–14711.
36 O. C. Compton, D. A. Dikin, K. W. Putz, L. C. Brinson and S. T. Nguyen, *Adv. Mater.*, 2010, **22**, 892–896.
37 Y. F. Li, Z. Zhou and L. B. Wang, *J. Chem. Phys.*, 2008, **129**.
38 B. Das, R. Voggu, C. S. Rout and C. N. R. Rao, *Chem. Commun.*, 2008, 5155–5157.
39 X. Y. Wang, X. F. Zhou, K. Yao, J. G. Zhang and Z. P. Liu, *Carbon*, 2011, **49**, 133–139.
40 J. Yao, X. P. Shen, B. Wang, H. K. Liu and G. X. Wang, *Electrochem. Commun.*, 2009, **11**, 1849–1852.
41 Y. M. Li, X. J. Lv, J. Lu and J. H. Li, *J. Phys. Chem. C*, 2010, **114**, 21770–21774.

